Supplementary information for - The physical meaning of charge extraction by linearly increasing voltage transients from organic solar cells

Robert Hanfland, Martin Andreas Fischer, Wolfgang Brütting,

Uli Würfel, Roderick C. I. MacKenzie*

*e-mail: roderick.mackenzie@nottingham.ac.uk

June 24, 2013

The supplementary information is divided in to two sections; section 1 describes supporting simulation results; and section 2 details simulation parameters.

1 Further results

1.1 Disorder

The charge distribution within a device during a CELIV transient: In Juška's original derivation of the CELIV method, he assumed band like transport and no dispersion. This meant that he could assume that, as the voltage transient was applied to the cell a uniform sheet of charge of density n (m^{-3}) was swept out from the device. This process produced a uniform depletion region of width $l(x)$ behind the charge sheet. The left hand side of figure 5 in the manuscript depicts this process. To investigate if this assumption holds when carrier traps are introduced into the device, a device with a very broad distribution of trap states (100 meV) was simulated. Figure S1 plots the electron density distribution in this device during a CELIV transient (only the electron profile has been plotted for brevity). It can be seen that, instead of a single sheet of charge

1

sliding across the device, as described in the derivation of the CELIV method, charge can be seen to reduce in magnitude equally over the entire device. This is because carriers are gradually detrapping from deeper and deeper energy states while the applied field sweeps detrapped carriers to the contacts. The reason for this progressive detrapping from ever deeper energy levels, is that during the application of the CELIV voltage ramp the quasi-Fermi level(s) of the free carriers will progressively move to lower energies forcing ever more deeply trapped states to release their carriers in order to move towards equilibrium, furthermore shallowly trapped carriers take less time to thermalize and become mobile than carriers in deeper traps. This process is shown in detail in figure S2, which plots energy space snapshots of the trapped electron distribution taken from the center of figure S1 at different stages during the CELIV transient. This process is summarized in the right hand side of figure 5 in the main body of the paper. This is the reason CELIV is not accurate in devices with high levels of disorder.
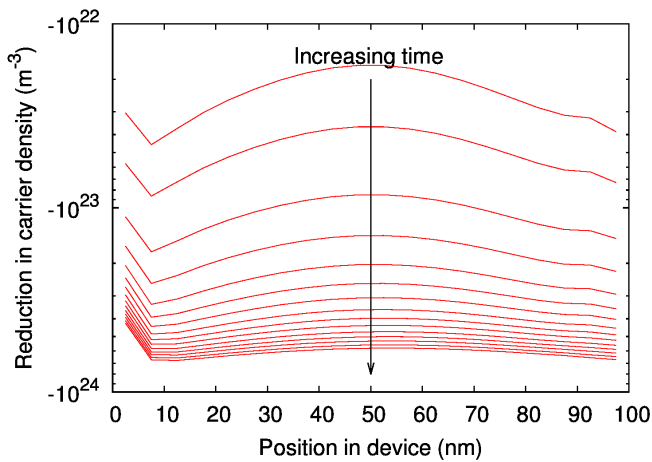
Figure S1: The reduction in the electron (free+trapped) carrier density across a device with a 100 meV tail slope during a CELIV measurement. The lines represent $2\mu s$ steps in time, starting $2\mu s$ after the beginning of the CELIV transient. It can be seen that the charge does not slides across the device as described in CE-LIV theory, instead it can be seen to reduce in magnitude equally over the entire device.
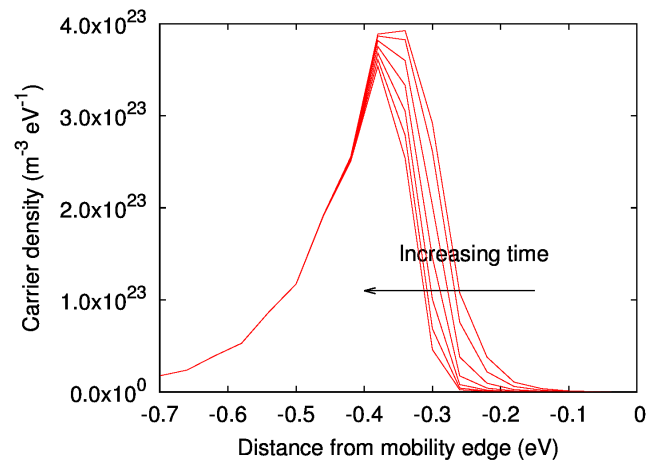
Figure S2: The time resolved electron distribution in energy space at 50 nm in figure S1) during the CELIV transient. Each line represents a $5\mu s$ step in time. It can be seen that carriers gradually detrap from deeper and deeper traps.

In contrast to figure S1, figure S3 plots the charge distribution during the CELIV transient for a device with very shallow trap states (25 meV). It can be seen that although the electron and hole populations do move to the contacts as a more negative bias is applied - as described in the derivation of CELIV. The charge distribution still does not conform to the idealized CELIV sheet of charge moving towards the contacts. This is because for a device with no trap states, the charge is distributed as an exponential function of position from one contact to the other; this is a reason why CELIV over estimates mobility for a device with no traps.
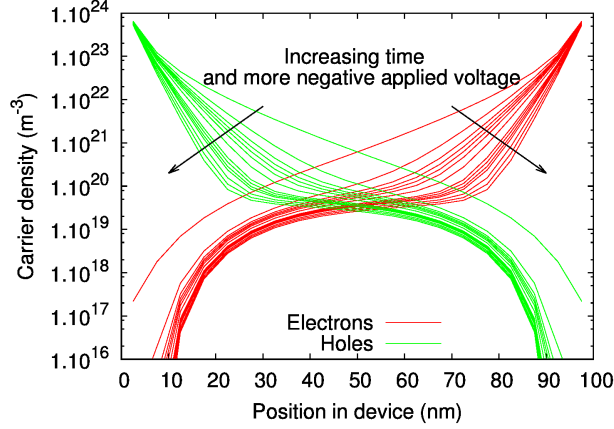
Figure S3: Distribution of carriers (trapped+free) in a device with very little disorder (tail slope of 25 meV) as a function of applied bias (0.5 V to -1.0 V). It can be seen that as a more negative bias is applied to the device, the center of the electron and hole charge distributions move towards the contacts. It is however far from the ideal CELIV extraction process of a sliding sheet of charge.

The influence of disorder on CELIV transients: Figure S4 plots five CELIV transients generated with different tail slope energies representing different levels of disorder in the material system. It can be seen that by changing only the level of disorder in the material, the peak of the CELIV transient can be shifted, and thus the mobility that would be measured with the CELIV method can be shifted from $4.2 \times 10^{-7} m^2 V^{-1} s^{-1}$ for a tail slope of 20 meV to $8.0 \times 10^{-10} m^2 V^{-1} s^{-1}$ for a tail slope of 80 meV. Increasing the number of trap states or the amount of disorder increases the maximum current produced during a CELIV transient because both these parameters increase the charge density within the device. Both trap density and disorder shift the peak of the CELIV transient to later times because in a device with more trap states or more disorder carriers are more likely to become trapped multiple times before reaching the contacts.
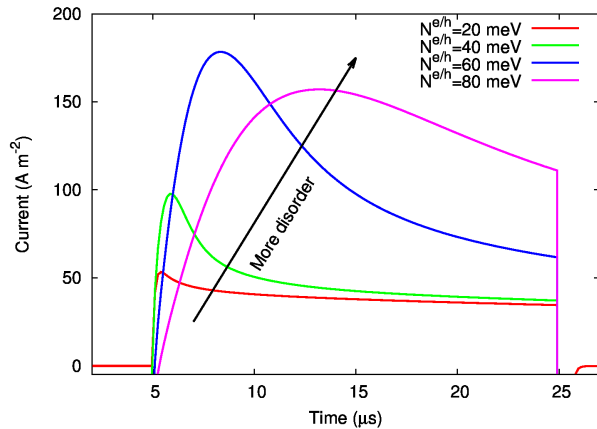
Figure S4: CELIV transients generated with varying levels of material disorder simulated by adjusting the tail slope energy.

3

1.2 Asymmetric carrier mobilities

Double peaks in CELIV transients: It has been suggested [L. Mattias Andersson, Fengling Zhang, Olle Ingans, Appl. Phys. Lett. 89 (2006) 142111] that for asymmetric mobilities a double peak should be observed in the CELIV transient. However, as can be seen from figure S5 no double peak was observed in the simulated results for asymmetric mobilities. The reason for this is that the magnitude of the maximum CELIV current was found to be far more sensitive to changes in mobility than the position of the peak. Thus the current due to the charge carrier with the higher mobility always dominated the transient and effectively hid the second peak of the charge carrier with the lower mobility. We also investigated asymmetric tail slopes, asymmetric carrier trapping/de-trapping rates, asymmetric recombination rates all of which did not produce a double CELIV peak. Indeed, the only way we were able to generate a second peak in the CELIV transient was to superimpose a single deep Gaussian trap on the exponential distribution of trap states at 0.5eV below the mobility edge. While it is possible that asymmetric mobilities could contribute to a double peak, our simulations suggest, asymmetric mobilities alone are not enough to cause them.
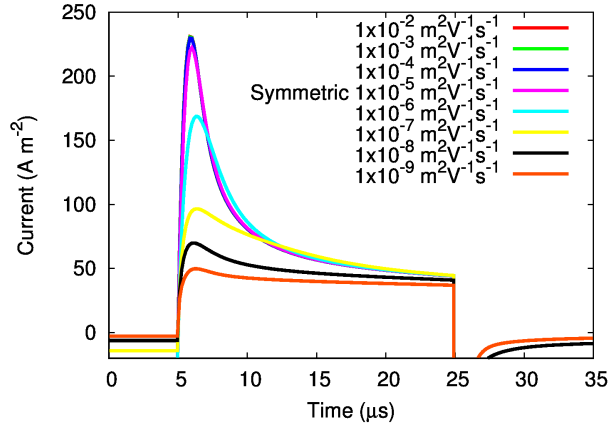
Figure S5: The influence of asymmetric mobilities on the shape of the CELIV transient. It can be seen that the magnitude of the CELIV transient moves far more than the position of the peak. This means that we do not observe two distinctive peaks. In this simulation the free hole mobility was kept at $\mu_h^0 = 1 \times 10^{-5}$ $m^2V^{-1}s^{-1}$ and the electron mobility varied.

Does CELIV measure the highest or lowest carrier mobility: Figures S6 plots the mobility extracted from CELIV transients against the electron and hole mobilities (calculated from equation 2), when the free carrier hole mobility is kept high ($\mu_h^0 = 1 \times 10^{-5} m^2V^{-1}s^{-1}$) and the free electron mobility varied. It can be seen that the CELIV method approximately gives the mobility of the most mobile charge carrier. From figure S7 it can be seen that when the free hole mobility is lowered to ($\mu_h^0 = 1 \times 10^{-7} m^2V^{-1}s^{-1}$) the CELIV mobility extracted from the transients is an average of the electron and hole mobilities.
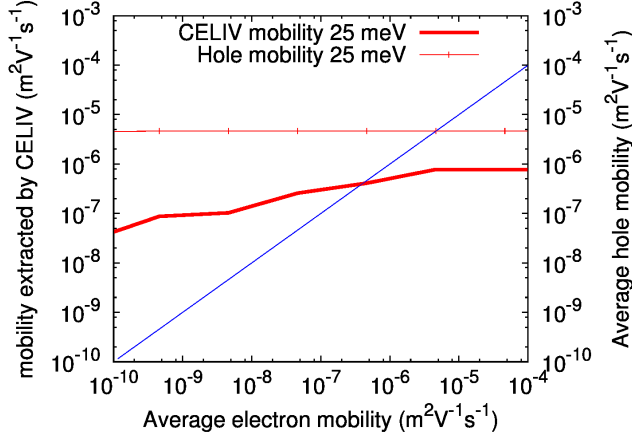
Figure S6: Extracted mobility from simulated CELIV transients using Juška's method, plotted against the device mobility calculated from equation 2 before the CELIV ramp is applied to the device. In this plot the free hole mobility is kept high at $\mu_h^0 = 1 \times 10^{-5} m^2 V^{-1} s^{-1}$ and the free electron mobility varied.
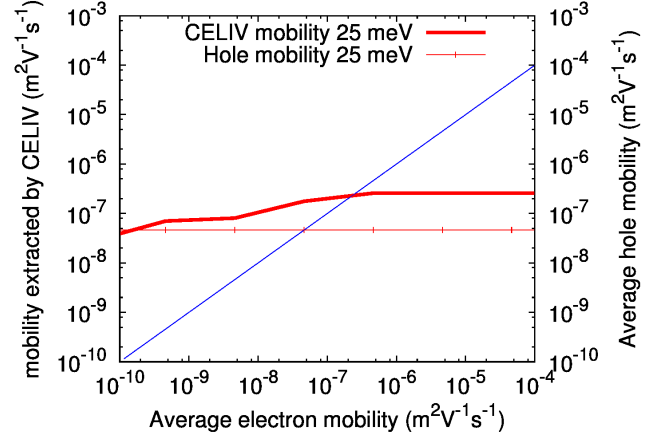
Figure S7: Extracted mobility from simulated CELIV transients using Juška's method, plotted against the device mobility calculated from equation 2 before the CELIV ramp is applied to the device. In this plot the free hole mobility is kept low at $\mu_h^0 = 1 \times 10^{-7} m^2 V^{-1} s^{-1}$ and the free electron mobility varied.

2 Simulation parameters

2.1 Generic simulation parameters

To generate figures 2, 3, and 4 device parameters were chosen which were symmetric and closely approximated what has been previously published [Phys. Rev. B 83, 115209 (2011)]. These parameters are given in table S1.

Mechanism	label	description
Density of electron trap states	5×10^{26}	$m^{-3}eV^{-1}$
Density of hole trap states	5×10^{26}	$m^{-3}eV^{-1}$
Free electron mobility	1×10^{-6}	$m^2V^{-1}s^{-1}$
Free hole mobility	1×10^{-6}	$m^2V^{-1}s^{-1}$
Electron-electron capture cross section	1×10^{-21}	m^2
Electron-hole capture cross section	1×10^{-22}	m^2
Hole-hole capture cross section	1×10^{-22}	m^2
Electron-hole capture cross section	1×10^{-21}	m^2
Density of carriers on the majority p-contact	1×10^{26}	m^{-3}
Density of carriers on the majority n-contact	1×10^{26}	m^{-3}
Effective density of states for free electrons	1×10^{26}	m^{-3}
Effective density of states for free holes	1×10^{26}	m^{-3}
Electron tail slope	50.00	meV
Hole tail slope	50.00	meV
Relative permittivity	3.0	
LUMO mobility edge	-3.80	eV
Effective band gap	1.10	eV
Thermal velocity	1×10^5	ms^{-1}
Shunt resistance	2×10^8	Ω
External series resistance	19.50	Ω
Cell thickness	100.0	nm

Table S1: Generic simulation parameters for the symmetric device

2.2   Modeling CELIV data of age and non aged solar cells

The model was fit to the experimental data using the down-hill-simplex method, device parameters were kept as close as possible to those previously published in the literature [Phys. Rev. B 83, 115209 (2011)]. Figures S8 and S9 show the result of the self consistent fit to the light and dark JV curves for the non-aged device; the fit of the CELIV transient is shown in the main body of the paper. The parameters which produce the figures S8, S9 and 1a are given in table S2.
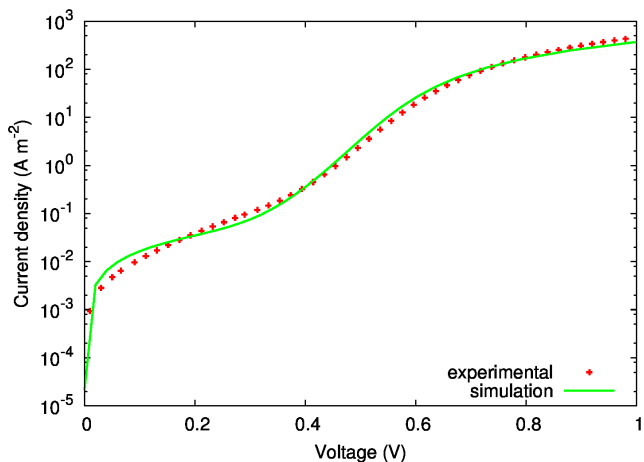
Figure S8: Simulated and experimental dark JV-curves for the non-aged device.
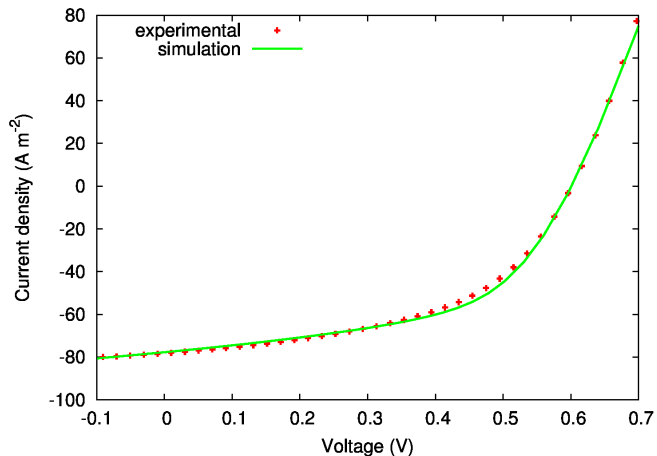
Figure S9: Simulated and experimental light JV-curves for the non-aged device.

Mechanism	label	description
Density of electron trap states	5.4×10^{25}	$m^{-3}eV^{-1}$
Density of hole trap states	5.4×10^{25}	$m^{-3}eV^{-1}$
Free electron mobility	1.8×10^{-7}	$m^2V^{-1}s^{-1}$
Free hole mobility	1×10^{-8}	$m^2V^{-1}s^{-1}$
Electron-electron capture cross section	3.9×10^{-22}	m^2
Electron-hole capture cross section	2.5×10^{-23}	m^2
Hole-hole capture cross section	7.3×10^{-25}	m^2
Electron-hole capture cross section	5×10^{-20}	m^2
Density of carriers on the majority p-contact	7.9×10^{26}	m^{-3}
Density of carriers on the majority n-contact	7.3×10^{26}	m^{-3}
Effective density of free electron states	1×10^{27}	m^{-3}
Effective density of free hole states	1×10^{27}	m^{-3}
Electron tail slope	51.20	meV
Hole tail slope	77.90	meV
Relative permittivity	3.00	
LUMO mobility edge	-3.80	eV
Effective band gap	1.10	eV
Thermal velocity	1×10^5	ms^{-1}
Shunt resistance	7.6×10^4	Ω
External series resistance	9.96	Ω
Cell thickness	220.0	nm

Table S2: Simulation parameters required to reproduce the non-aged CELIV transient, note only the trap densities (N_e^{exp} and N_h^{exp}) were changed to fit the aged CELIV transient.

The aged device had identical parameters except for the density of electron (hole) trap states

which were $1.9 \times 10^{26} (1.8 \times 10^{26}) m^{-3} eV^{-1}$.

2.3   Simulating CELIV transients

To simulate CELIV transients the parasitic shunt/series resistances and the geometric capacitance of the diode must be taken into account to calculate the boundary conditions for Possion's equation. To do this Kirchoff's current laws are applied to the resistor-capacitor network representing the parasitic components of the solar cell. The resulting equations are solved simultaneously and self consistently within the same newton solver used to solve Possion's, the drift-diffusion and the Shockley-Read-Hall capture escape equations. Although it was found possible to solve the parasitic network externally from the main newton solver it was found inefficient and unstable.